

# Extracting strange quark freeze-out information in Pb+Pb collisions at $\sqrt{s_{NN}}=2.76$ TeV from $\phi$ and $\Omega$ production

Jie Pu,<sup>1</sup> Kai-Jia Sun,<sup>1</sup> and Lie-Wen Chen\*<sup>1</sup>

<sup>1</sup>*School of Physics and Astronomy and Shanghai Key Laboratory for Particle Physics and Cosmology, Shanghai Jiao Tong University, Shanghai 200240, China*

(Dated: March 16, 2022)

Using a covariant quark coalescence model combined with a blast-wave-like analytical parametrization for (anti-)strange quark phase-space freeze-out configuration, we extract information on strange quark freeze-out dynamics in Pb+Pb collisions at  $\sqrt{s_{NN}}=2.76$  TeV by fitting the measured transverse momentum spectra and elliptic flows ( $v_2$ ) of  $\phi$  mesons and  $\Omega$  baryons. We find that although both the measured and calculated  $v_2$  of  $\phi$  and  $\Omega$  satisfy the number-of-constituent-quark (NCQ) scaling, the NCQ-scaled  $v_2$  is significantly smaller than the  $v_2$  of strange quarks, implying that the NCQ-scaled  $v_2$  of  $\phi$  and  $\Omega$  cannot be simply identified as the  $v_2$  of strange quarks at hadronization. Meanwhile, our results indicate that the covariant quark coalescence model can nicely describe the spectra and elliptic flows of  $\phi$  and  $\Omega$  simultaneously, suggesting the coalescence mechanism is still valid for  $\phi$  and  $\Omega$  production in Pb+Pb collisions at LHC energies.

## I. INTRODUCTION

The main goal of relativistic heavy-ion collisions, including those being carried out at Relativistic Heavy-Ion Collider (RHIC) and Large Hadron Collider (LHC), is to explore the Quantum Chromodynamics (QCD) phase diagram, especially the properties of deconfined quark-gluon plasma (QGP) that could be created in these collisions and its transition to hadronic matter [1, 2]. Results of *ab initio* lattice QCD (LQCD) simulations [3–7] and effective model approaches [8, 9] have provided important insights on the QCD phase diagram. Experimentally, however, the QGP cannot be probed directly since partons are confined to form hadrons via hadronization during the dynamical evolution of heavy-ion collisions. Therefore, it is particularly important to study the production of some special particles which have small final hadronic interactions and thus could carry important information on the early QGP dynamics in relativistic heavy-ion collisions. The multistrange hadrons, e.g., the  $\phi$  meson which carries hidden strangeness ( $s\bar{s}$ ) and the  $\Omega$  baryon which consists of three valence strange quarks ( $sss$ , i.e.,  $\Omega^-$ ) or anti-strange quarks ( $\bar{s}\bar{s}\bar{s}$ , i.e.,  $\Omega^+$ ), are such particles, because they have small hadronic interaction cross sections and are little affected by re-scattering effects in later hadronic stage of the collisions [10–16]. Furthermore, since both  $\phi$  meson and  $\Omega$  baryon consist solely of (anti-)strange quarks, their production thus provides an ideal probe to extract the strange quark freeze-out information at hadronization in relativistic heavy-ion collisions.

The masses of strange quarks are comparable to the temperature of the QGP and they are thus expected to be abundantly produced from quark and gluon inelastic scattering in the QGP, and the strangeness enhancement

is thus proposed as one of the signatures for the QGP formation in relativistic heavy-ion collisions [17, 18]. In the past decades, strangeness production in relativistic heavy-ion collisions has been a topic of great interest and significant progress has been made in understanding the strangeness dynamics and the QGP properties (see, e.g., Refs. [19–21] for recent review).

Compared to the yield and invariant transverse momentum spectrum, the elliptic flow ( $v_2$ ), which is the second Fourier coefficient of the azimuthal distribution of the emitted particles [22, 23], is more sensitive to the early stage dynamics of heavy-ion collisions [24–27]. Of particular interest is that the observed elliptic flows of identified hadrons in heavy-ion collisions at RHIC and LHC were found to satisfy the number-of-constituent-quark (NCQ) scaling; that is, the elliptic flow per quark is the same at the same transverse momentum per quark. As shown in Refs. [28–31], such a scaling of hadron elliptic flows according to their constituent quark numbers can be understood via a unique hadronization mechanism, i.e., the quark recombination/coalescence. The quark coalescence mechanism is also supported by the observed anomalously large enhancement of baryon to meson ratio at intermediate transverse momenta [28–32] as well as the scaling relations observed among higher-order hadron anisotropic flows [33–36]. These findings provide a strong indication that the quark degrees of freedom are dominant at the time of hadronization and the partonic collectivity has been developed during the partonic evolution prior to hadronization.

The production of  $\phi$  mesons and  $\Omega$  baryons in relativistic heavy-ion collisions has been extensively investigated in the past decades [12, 37–53], and this has significantly deepened our understanding on the strangeness dynamics and the QGP properties. Although the elliptic flow of parton degrees of freedom cannot be directly measured experimentally, the NCQ-scaled elliptic flow of hadrons is believed to reflect that of the constituent quarks at hadronization. In fact, according to the naive

---

\*Corresponding author: lwchen@sjtu.edu.cn

momentum-space quark coalescence model [30, 35, 36] in which only the quarks with equal momentum are allowed to coalesce, the obtained NCQ-scaled  $v_2$  of hadrons should be equal to  $v_2$  of the constituent quarks. On the other hand, a more realistic dynamical quark coalescence model [37] which is based on the quark phase-space information from a multiphase transport (AMPT) model [54] has been used to study the production and anisotropic flows of  $\phi$  and  $\Omega$  in Au+Au collisions at RHIC energies, and it is found that the NCQ-scaled  $v_2$  of  $\phi$  and  $\Omega$  are significantly smaller than that of strange quarks. However, that work is failed to describe the transverse momentum spectra of  $\phi$  and  $\Omega$  [37].

In addition, although the  $v_2$  of  $\phi$  mesons nicely follows the constituent quark number scaling in Au+Au collisions at RHIC energies, the scaling tends to be violated in Pb+Pb collisions at LHC energies based on the measured  $v_2$  of  $\phi$  mesons and protons [44], and this causes the discussion about if the quark coalescence as a relevant particle production mechanism is still valid or not in heavy-ion collisions at LHC energies [51]. Therefore, it is interesting to see if both the spectra and elliptic flows of  $\phi$  and  $\Omega$  in Pb+Pb collisions at LHC energies can be simultaneously described within a more realistic quark coalescence model, and thus to explore the possibility of quantitatively extracting the strange quark freeze-out information at hadronization from the measured data of  $\phi$  and  $\Omega$ . This is the main motivation of the present work.

In this work, we extend the covariant coalescence model [55] combined with a blast-wave-like [56] analytical parametrization for constituent particle phase-space freeze-out configuration, which has been successfully applied recently to describe the (anti-)light-(hyper)nuclei production in relativistic heavy-ion collisions via (anti-)nucleon (and/or hyperon) coalescence [57–59], to describe the transverse momentum spectra and elliptic flows of  $\phi$  and  $\Omega$  in Pb+Pb collisions at  $\sqrt{s_{NN}}=2.76$  TeV via quark coalescence. Our results indicate that the quark coalescence model can nicely describe both the spectra and elliptic flows of  $\phi$  and  $\Omega$  simultaneously, suggesting the quark coalescence mechanism is still valid for  $\phi$  and  $\Omega$  production in Pb+Pb collisions at LHC energies. We also find that both the measured and calculated  $v_2$  of  $\phi$  and  $\Omega$  satisfy the NCQ scaling, but the NCQ-scaled  $v_2$  is significantly smaller than the  $v_2$  of strange quarks by a factor of about 1.35 in centrality 10 – 20% Pb+Pb collisions at  $\sqrt{s_{NN}} = 2.76$  TeV. Furthermore, the strange quark freeze-out information is obtained.

The paper is organized as follows: In Sec. II, we introduce the covariant coalescence model combined with a blast-wave-like analytical parametrization for (anti-)strange quark phase-space freeze-out configuration. We then apply the model to describe the transverse momentum spectra and elliptic flows of  $\phi$  and  $\Omega^-$  in centrality 10 – 20% Pb+Pb collisions at  $\sqrt{s_{NN}} = 2.76$  TeV, and then the obtained results are presented and discussed in Sec. III. Finally, we summarize our conclusions in Sec IV.

## II. MODEL AND METHOD

In this work, the covariant coalescence model [55] combined with a blast-wave-like analytical parametrization [56] for (anti-)strange quark phase-space freeze-out configuration is used to describe the production of  $\phi$  and  $\Omega$  in relativistic heavy-ion collisions. In particular, for  $\phi$  and  $\Omega$  production at mid-rapidity in Pb+Pb collisions at  $\sqrt{s_{NN}} = 2.76$  TeV considered here, we assume a longitudinal boost-invariant expansion for the (anti-)strange quarks and the Lorentz invariant one-particle momentum distribution is then given by

$$E \frac{d^3 N}{d^3 p} = \frac{d^3 N}{p_T dp_T d\phi_p dy} = \int d^4 x S(x, p), \quad (1)$$

where  $S(x, p)$  is the emission function and it is taken to be a blast-wave-like parametrization as [56]

$$S(x, p) d^4 x = m_T \cosh(\eta - y) f(x, p) J(\tau) d\tau d\eta dr d\phi_s. \quad (2)$$

In above expressions, we use longitudinal proper time  $\tau = \sqrt{t^2 - z^2}$ , spacetime rapidity  $\eta = \frac{1}{2} \ln \frac{t-z}{t+z}$ , cylindrical coordinates  $(r, \phi_s)$ , rapidity  $y = \frac{1}{2} \ln \left( \frac{E+p_z}{E-p_z} \right)$ , transverse momentum  $(p_T, \phi_p)$ , and transverse mass  $m_T = \sqrt{m^2 + p_T^2}$ . The statistical distribution function  $f(x, p)$  is given by

$$f(x, p) = g(2\pi)^{-3} [\exp(p^\mu u_\mu / kT) / \xi \pm 1]^{-1}, \quad (3)$$

where  $g$  is statistical degeneracy factor including spin and color degrees of freedom,  $p^\mu$  is the four-momentum of the emitted particle,  $u_\mu$  is the four-velocity of a fluid element in the fireball,  $T$  is the local temperature and  $\xi$  is the fugacity. The  $p^\mu u_\mu$  is the energy in the local rest frame of the fluid and reads

$$p^\mu u_\mu = m_T \cosh \rho \cosh(\eta - y) - p_T \sinh \rho \cos(\phi_p - \phi_b), \quad (4)$$

where  $\rho$  is the transverse rapidity distribution (transverse flow profile) of the fluid element in the fireball,  $\phi_p$  is azimuthal direction of the emitted particle, and  $\phi_b$  is azimuthal direction of the transverse flow which is different from the spatial azimuthal angle  $\phi_s$ . We also assume the freeze-out proper time follows a Gaussian distribution [56]

$$J(\tau) = \frac{1}{\Delta\tau\sqrt{2\pi}} \exp\left(-\frac{(\tau - \tau_0)^2}{2(\Delta\tau)^2}\right) \quad (5)$$

with a mean value  $\tau_0$  and a dispersion  $\Delta\tau$ . More detailed information can be found in Refs. [57–59].

In order to improve the description on the measured  $\phi$  and  $\Omega$  elliptic flows at higher transverse momenta ( $p_T \gtrsim 2$  GeV/c), an  $r$ -dependent coefficient  $c_1 \exp(-r^2/c_2^2)$  is introduced in the transverse rapidity flow profile, and the flow profile is parameterized as

$$\rho = \rho_0 \tilde{r} \left[ 1 + c_1 e^{-\frac{r^2}{c_2^2}} \cos(2\phi_b) \right], \quad (6)$$

where  $\rho_0$  is the isotropic part of the transverse rapidity flow,  $c_1$  is introduced to describe anisotropy of transverse flow,  $c_2$  denotes a suppression of anisotropy at larger  $r$  where the (anti-)strange quarks in the local cell have a larger averaged value of  $p_T$  due to the larger transverse velocity of the cell in the fireball, and  $\tilde{r}$  is the ‘‘normalized elliptical radius’’ [56]

$$\tilde{r} = \sqrt{\frac{[r \cos \phi_s]^2}{R_x^2} + \frac{[r \sin \phi_s]^2}{R_y^2}}, \quad (7)$$

where  $R_x = R_0(1 + s_2)$  is the minor axis of the ellipse,  $R_y = R_0(1 - s_2)$  is the major axis, and  $s_2$  denotes the geometric anisotropy.  $R_0$  is the transverse radius of the fireball. The phase-space freeze-out configuration of the constituent particles are thus determined by nine parameters:  $T$ ,  $\rho_0$ ,  $R_0$ ,  $\tau_0$ ,  $\Delta\tau$ ,  $\xi$ ,  $c_1$ ,  $c_2$ ,  $s_2$ .

The Lorentz invariant one-particle momentum distribution can be decomposed as [22, 23]

$$\begin{aligned} E \frac{d^3 N}{d^3 p} &= \frac{d^3 N}{p_T dp_T d\phi_p dy} \\ &= \frac{1}{2\pi} \frac{d^2 N}{p_T dp_T dy} \left[ 1 + \sum_{n=1}^{\infty} 2v_n(p_T, y) \cos(n\phi_p) \right], \end{aligned} \quad (8)$$

where  $v_n$  denotes the anisotropic flows:

$$v_n = \langle \cos(n\phi_p) \rangle = \frac{\int \frac{d^3 N}{d^2 p_T dy} \cos(n\phi_p) d\phi_p}{\int \frac{d^3 N}{d^2 p_T dy} d\phi_p}. \quad (9)$$

The famous elliptic flow ( $v_2$ ) corresponds to the second Fourier coefficient of the azimuthal distribution of the emitted particles.

With the above phase-space freeze-out information for constituent particles, we can use the covariant coalescence model to calculate the invariant momentum distribution of clusters. In the coalescence model, the probability for producing a cluster is determined by the overlap of its Wigner phase-space density (Wigner function) with the constituent particle phase-space distribution at freeze-out. If  $M$  particles are coalesced into a cluster, the invariant differential transverse momentum distribution of the cluster can be obtained as

$$\begin{aligned} E \frac{d^3 N_c}{d^3 P} &= E g_c \int \left( \prod_{i=1}^M \frac{d^3 p_i}{E_i} d^4 x_i S(x_i, p_i) \right) \times \\ &\rho_c^W(x_1, \dots, x_M; p_1, \dots, p_M) \delta^3 \left( \mathbf{P} - \sum_{i=1}^M \mathbf{p}_i \right), \end{aligned} \quad (10)$$

where  $N_c$  is the cluster multiplicity,  $E(\mathbf{P})$  is its energy (momentum),  $\delta$ -function is adopted to ensure momentum conservation,  $g_c$  is the coalescence factor including the spin and color degrees of freedom and is expressed as  $g_c = \frac{2J+1}{2M^3}$  [60], and  $\rho_c^W$  is the Wigner function of the

cluster. In this work, the harmonic oscillator wave functions are assumed for the cluster and its Wigner function is

$$\begin{aligned} &\rho_c^W(x_1, \dots, x_M; p_1, \dots, p_M) \\ &= \rho^W(q_1, \dots, q_{M-1}, k_1, \dots, k_{M-1}) \\ &= 8^{M-1} \exp \left[ - \sum_{i=1}^{M-1} (q_i^2 / \sigma_i^2 + \sigma_i^2 k_i^2) \right], \end{aligned} \quad (11)$$

where  $\sigma_i^2 = (\mu_i w)^{-1}$ ,  $\mu_{i-1} = \frac{i}{i-1} \frac{m_i \sum_{k=1}^{i-1} m_k}{\sum_{k=1}^{i-1} m_k}$  ( $i \geq 2$ ) is the reduced mass in the center-of-mass frame,  $q_i = \sqrt{\frac{i}{i+1}} (\frac{\sum_{k=1}^i m_k x_k}{\sum_{k=1}^i m_k} - x_{i+1})$  is the relative coordinate,  $k_i$  is the relative momentum, and  $w$  is the harmonic oscillator frequency which is related to the root-mean-square radius of the cluster as follows [57]

$$\langle r_M^2 \rangle = \frac{3}{2Mw} \left[ \sum_{i=1}^M \frac{1}{m_i} - \frac{M}{\sum_{i=1}^M m_i} \right]. \quad (12)$$

The integral (10) can be directly calculated through multi-dimensional numerical integration by Monte-Carlo method [57, 61]. The cluster elliptic flow can be calculated from Eq. (9) and Eq. (10). It should be emphasized that since the constituent particles may have different freeze-out time, in the numerical calculation, the constituent particles that freeze out earlier are allowed to propagate freely until the time when the last constituent particle in the cluster freezes out in order to make the coalescence at equal time in the rest frame of the cluster [37, 57, 62].

### III. RESULT AND DISCUSSION

By using the model and method introduced above, we can extract the phase-space freeze-out information, namely,  $T$ ,  $\rho_0$ ,  $R_0$ ,  $\tau_0$ ,  $\Delta\tau$ ,  $\xi$ ,  $c_1$ ,  $c_2$  and  $s_2$ , of (anti-)strange quarks in Pb+Pb collisions at  $\sqrt{s_{NN}} = 2.76$  TeV by fitting the experimental data on  $\phi$  and  $\Omega$  production. In the following, the mass of (anti-)strange quark is taken to be 500 MeV, and the root-mean-square radii of  $\phi$  and  $\Omega$  are taken to be 0.87 fm and 1.0 fm [63], respectively. The coalescence factors  $g_c$  including spin and color degrees of freedom are  $3/(3^2 \times 2^2)$  and  $4/(3^3 \times 2^3)$  for  $\phi$  and  $\Omega$ , respectively. The details can be found in Ref. [63]. In addition, in the present work, the anti-strange quarks are assumed to have the same freeze-out parameters as strange quarks because the  $\bar{\Omega}^+/\Omega^-$  ratio is close to unity in Pb+Pb collisions at  $\sqrt{s_{NN}} = 2.76$  TeV [42].

By fitting the transverse momentum spectra and elliptic flows of  $\phi$  and  $\Omega^-$  [42–44] in centrality 10–20% Pb+Pb collisions at  $\sqrt{s_{NN}} = 2.76$  TeV simultaneously, the parameters of (anti-)strange quark phase-space freeze-out configurations are extracted and summarized as FOPb-s (Freeze-Out in  $\mathbf{Pb}+\mathbf{Pb}$  collisions for strange

TABLE I: Parameters of the blast-wave-like analytical parametrization for mid-rapidity (anti-)strange quark phase-space freeze-out configurations in centrality 10 – 20% Pb+Pb collisions at  $\sqrt{s_{NN}} = 2.76$  TeV.

	$T(\text{MeV})$	$\rho_0$	$R_0(\text{fm})$	$\tau_0(\text{fm}/c)$	$\Delta\tau(\text{fm}/c)$	$\xi_s$
FOPb-s	154	1.06	14.8	13.0	1.3	0.78
	$c_1$	$c_2(\text{fm})$	$s_2$			
FOPb-s	0.38	8.7	-0.05			

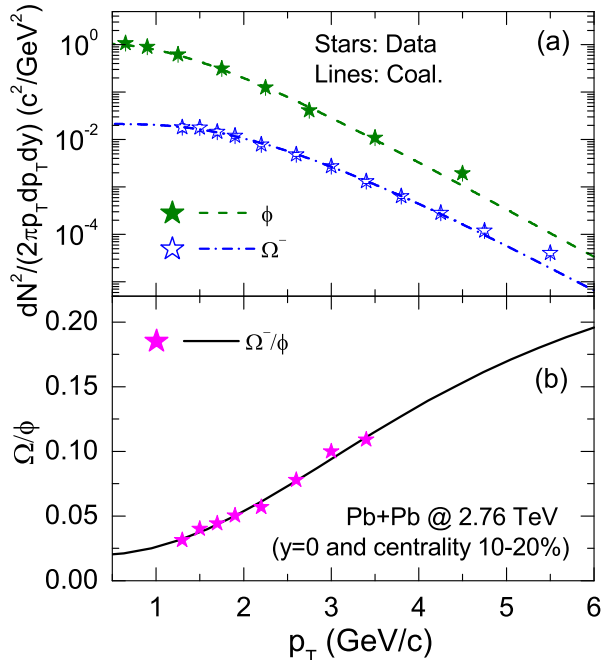


FIG. 1: (Color online) Transverse momentum distribution of mid-rapidity  $\phi$  mesons and  $\Omega^-$  baryons in centrality 10 – 20% Pb+Pb collisions at  $\sqrt{s_{NN}}=2.76$  TeV (a) and the corresponding yield ratio of  $\Omega^-$  baryons to  $\phi$  mesons (b). The lines are from the quark coalescence model predictions and the stars are experimental data taken from ALICE measurement [42, 43].

quarks) shown in Table I. Here the local temperature is fixed as  $T = 154$  MeV following the QCD transition temperature obtained from the high-precision studies of the chiral and deconfinement aspects of the QCD transition at zero baryon chemical potential [5], and the extracted transverse flow parameter is  $\rho_0 = 1.06$ , transverse radius is  $R_0 = 14.8$  fm, the longitudinal proper time is  $\tau_0 = 13.0$  fm/c, the time dispersion is  $\Delta\tau = 1.3$  fm/c, the fugacity of (anti-)strange quark is 0.78, the geometric anisotropy is  $s_2 = -0.05$  and the anisotropy parameters are  $c_1 = 0.38$  and  $c_2 = 8.7$  fm. These parameters give a quantitative description about the (anti-)strange quark phase-space freeze-out configuration for centrality 10 – 20% Pb+Pb collisions at  $\sqrt{s_{NN}} = 2.76$  TeV.

Shown in Fig. 1 (a) are the experimental data and theoretical calculations for the transverse momentum spec-

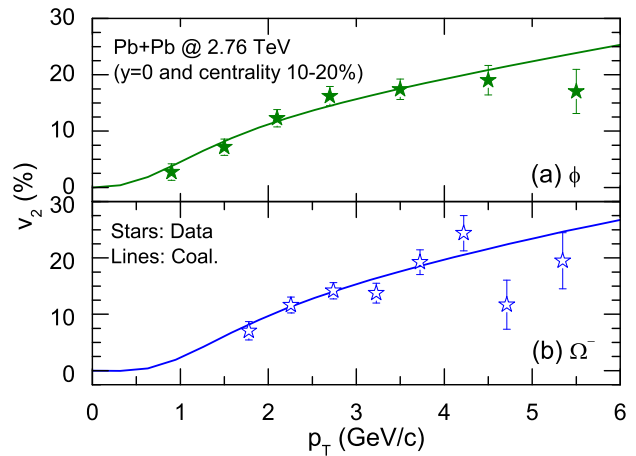


FIG. 2: (Color online) The measured (stars) and calculated (lines) transverse momentum dependence of the elliptic flows ( $v_2$ ) for mid-rapidity  $\phi$  mesons (a) and  $\Omega^-$  baryons (b) in centrality 10 – 20% Pb+Pb collisions at  $\sqrt{s_{NN}}=2.76$  TeV. The experimental results (stars) are taken from ALICE measurement [44].

tra of  $\phi$  and  $\Omega^-$  in centrality 10 – 20% Pb+Pb collisions at  $\sqrt{s_{NN}} = 2.76$  TeV. The corresponding results on the yield ratio of  $\Omega^-$  baryons to  $\phi$  mesons as a function of transverse momentum are shown in Fig. 1 (b). The experimental data are taken from ALICE measurement [42, 43]. It is seen that the present coalescence model predictions are in good agreement with the experimental data from ALICE measurements. In particular, the  $\Omega^-/\phi$  ratio enhances with the transverse momentum, e.g., its value changes from about 0.02 at  $p_T = 0.5$  GeV/c to about 0.1 at  $p_T = 3$  GeV/c, with an enhancement factor of about 5. This enhancement can be understood as a result of quark coalescence mechanism [28–32] as in the case of observed anomalously large anti-proton to pion ratio in central and mid-peripheral (centrality of about 30%) Au+Au collisions at  $\sqrt{s_{NN}} = 200$  GeV [64]. It should be pointed out that the enhancement can be also explained by the mass effect (the  $\Omega$  is heavier than the  $\phi$ ) via fitting the data with a Boltzmann-Gibbs blast-wave function [43, 65].

Figure 2 shows the experimental data and theoretical calculations on the transverse momentum dependence of the elliptic flows of  $\phi$  and  $\Omega^-$  in centrality 10 – 20% Pb+Pb collisions at  $\sqrt{s_{NN}}=2.76$  TeV. The experimental data are taken from the ALICE measurement [44]. One sees that the present quark coalescence model can nicely describe the experimental data. From Fig. 1 and Fig. 2, it is seen that both the transverse momentum spectra and elliptic flows of  $\phi$  and  $\Omega^-$  can be described very well in the present covariant quark coalescence model with the same parameter set FOPb-s, which provides important information on the phase-space freeze-out configuration of mid-rapidity (anti-)strange quarks in centrality 10 – 20% Pb+Pb collisions at  $\sqrt{s_{NN}}=2.76$  TeV. Our results demonstrate that the quark coalescence mechanism

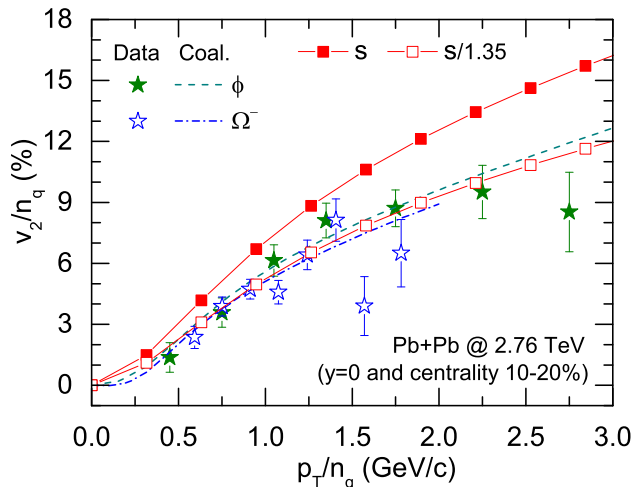


FIG. 3: (Color online) NCQ-scaled elliptic flow ( $v_2/n_q$ ) as a function of scaled transverse momentum ( $p_T/n_q$ ) for mid-rapidity  $\phi$  mesons and  $\Omega^-$  baryons in centrality 10 – 20% Pb+Pb collisions at  $\sqrt{s_{NN}}=2.76$  TeV. Also shown are the corresponding results from quark coalescence model predictions (dashed and dash-dotted lines) as well as the results for (anti-)strange quarks at freeze-out (solid squares) and their scaled values (divided by a factor of 1.35) (open squares). The experimental data (stars) are taken from ALICE measurement [44].

is still valid for  $\phi$  and  $\Omega$  production in Pb+Pb collisions at LHC energies. The observed violation of the NCQ scaling for the  $v_2$  of  $\phi$  mesons and protons in Pb+Pb collisions at LHC energies [44] probably is due to the different final hadronic interactions for  $\phi$  mesons and protons in heavy-ion collisions at LHC energies.

Figure 3 shows the measured and calculated NCQ-scaled elliptic flow  $v_2/n_q$  as a function of scaled transverse momentum  $p_T/n_q$  for mid-rapidity  $\phi$  and  $\Omega$  in centrality 10 – 20% Pb+Pb collisions at  $\sqrt{s_{NN}}=2.76$  TeV. Also included in Fig. 3 are the corresponding results for (anti-)strange quarks at freeze-out as well as their scaled values (divided by a factor of 1.35). It is seen that the measured and calculated elliptic flows of  $\phi$  and  $\Omega$  approximately satisfy the famous NCQ scaling relation. However, the NCQ-scaled elliptic flows of  $\phi$  and  $\Omega$  are significantly smaller than that of the coalescing (anti-)strange quarks. More quantitatively, we find that the elliptic flow of (anti-)strange quarks is about 1.35 times the NCQ-scaled elliptic flows of  $\phi$  and  $\Omega$ . This is different from the prediction of the naive momentum-space quark coalescence model [30, 35, 36] in which only the quarks with equal momentum are allowed to coalesce. In this simple model, the momentum spectrum of  $\phi$  meson is proportional to the product of the momentum spectra of strange and anti-strange quarks, leading to the result that the NCQ-scaled elliptic flow  $v_2/n_q$  of  $\phi$  mesons equals to the  $v_2$  of (anti-)strange quarks, which can be demonstrated from a simple Fourier analysis [30, 35, 36]. The same conclusion is also obtained in the case of  $\Omega$

baryons. Therefore, in the naive momentum-space quark coalescence model, the obtained NCQ-scaled  $v_2$  of  $\phi$  and  $\Omega$  should be equal to  $v_2$  of (anti-)strange quarks.

Unlike the naive momentum-space quark coalescence model, in the present covariant quark coalescence model, the effects of finite sizes of hadrons and nonzero relative momenta of partons inside the hadrons have been encoded in the hadron Wigner function in full phase-space and thus quarks with unequal momenta can be coalesced into hadrons ( $\phi$  and  $\Omega$ ), and this may smear the azimuthal distribution of the formed hadrons and thus leads to a suppression of hadron elliptic flows. The magnitude of the suppression is directly related to the internal structure and size of the hadrons. Although this phenomenon has actually been observed in previous work [37] within a dynamical quark coalescence model using the parton freeze-out information based on the AMPT transport model calculations, the transverse momentum spectra of  $\phi$  and  $\Omega$  were failed to be reproduced there. Our results indicate that the NCQ-scaled elliptic flows of  $\phi$  and  $\Omega$  significantly underestimate the elliptic flow of (anti-)strange quarks and they cannot be simply identified as the elliptic flow of the (anti-)strange quarks in relativistic heavy-ion collisions.

#### IV. CONCLUSION

Based on the covariant quark coalescence model with a blast-wave-like analytical parametrization for the phase-space configuration of mid-rapidity (anti-)strange quarks at freeze-out, we have extracted information of strange quark freeze-out dynamics in centrality 10 – 20% Pb+Pb collisions at  $\sqrt{s_{NN}}=2.76$  TeV by simultaneously fitting the transverse momentum spectra and elliptic flows of  $\phi$  and  $\Omega$ . We have found that our model can successfully describe the experimental data on both the transverse momentum spectra and elliptic flows of  $\phi$  and  $\Omega$ , demonstrating that the quark coalescence mechanism is still valid for  $\phi$  and  $\Omega$  production in heavy-ion collisions at LHC energies.

Our results indicate that the measured and calculated elliptic flows of  $\phi$  and  $\Omega$  approximately satisfy the famous NCQ scaling relation, but unlike the prediction of the naive momentum-space quark coalescence model, the NCQ-scaled elliptic flows of  $\phi$  and  $\Omega$  are significantly smaller than that of the coalescing (anti-)strange quarks, with the latter being about 1.35 times the former. This means that one cannot simply identify the experimentally measured NCQ-scaled elliptic flows of  $\phi$  and  $\Omega$  as the elliptic flow of (anti-)strange quarks in relativistic heavy-ion collisions.

The present work provides useful information on the strangeness freeze-out dynamics in relativistic heavy-ion collisions. The model and method in the present work can be further applied to heavy-ion collisions at energies of beam energy scan (BES) program at STAR/RHIC. Such studies are in progress and will be reported else-

where.

### Acknowledgments

The authors thank Professor Che Ming Ko for helpful discussions. This work was supported in part by the National Natural Science Foundation of China under Grant

No. 11625521, the Major State Basic Research Development Program (973 Program) in China under Contract No. 2015CB856904, the Program for Professor of Special Appointment (Eastern Scholar) at Shanghai Institutions of Higher Learning, Key Laboratory for Particle Physics, Astrophysics and Cosmology, Ministry of Education, China, and the Science and Technology Commission of Shanghai Municipality (11DZ2260700).

- 
- [1] B.V. Jacak and B. Müller, *Science* **337**, 310 (2012).  
 [2] E. Shuryak, *Rev. Mod. Phys.* **89**, 035001 (2017).  
 [3] Y. Aoki, G. Endrodi, Z. Fodor, S.D. Katz, and K.K. Szabo, *Nature* **443**, 675 (2006).  
 [4] H.-T. Ding, F. Karsch, and S. Mukherjee, *Int. J. Mod. Phys. E* **24**, 1530007 (2015).  
 [5] A. Bazavov, T. Bhattacharya, M. Cheng, C. DeTar, H. T. Ding, S. Gottlieb, R. Gupta, P. Hegde, U. M. Heller, F. Karsch, E. Laermann, L. Levkova, S. Mukherjee, P. Petreczky, C. Schmidt, R. A. Soltz, W. Soeldner, R. Sugar, D. Toussaint, W. Unger, and P. Vranas, *Phys. Rev. D* **85**, 054503 (2012).  
 [6] A. Bazavov, T. Bhattacharya, C. DeTar, H. T. Ding, S. Gottlieb, R. Gupta, P. Hegde, U. M. Heller, F. Karsch, E. Laermann, L. Levkova, S. Mukherjee, P. Petreczky, C. Schmidt, C. Schroeder, R. A. Soltz, W. Soeldner, R. Sugar, M. Wagner, and P. Vranas, *Phys. Rev. D* **90**, 094503 (2014).  
 [7] A. Bazavov, H.-T. Ding, P. Hegde, O. Kaczmarek, F. Karsch, E. Laermann, Y. Maezawa, S. Mukherjee, H. Ohno, P. Petreczky, H. Sandmeyer, P. Steinbrecher, C. Schmidt, S. Sharma, W. Soeldner, and M. Wagner, *Phys. Rev. D* **95**, 054504 (2017).  
 [8] K. Fukushima and T. Hatsuda, *Rep. Prog. Phys.* **74**, 014001 (2011).  
 [9] P. Braun-Munzinger, V. Koch, T. Schäfer, and J. Stachel, *Phys. Rep.* **621**, 76 (2016).  
 [10] A. Shor, *Phys. Rev. Lett.* **54**, 1122 (1985).  
 [11] C.P. Singh, *Phys. Rev. Lett.* **56**, 1750 (1986).  
 [12] H. van Hecke, H. Sorge, and N. Xu, *Phys. Rev. Lett.* **81**, 5764 (1998).  
 [13] S.A. Bass, A. Dumitru, M. Bleicher, L. Bravina, E. Zabrodin, H. Stöcker, and W. Greiner, *Phys. Rev. C* **60**, 021902(R) (1999); A. Dumitru, S.A. Bass, M. Bleicher, H. Stöcker, and W. Greiner, *Phys. Lett. B* **460**, 411 (1999); S.A. Bass and A. Dumitru, *Phys. Rev. C* **61**, 064909 (2000).  
 [14] Y. Cheng, F. Liu, Z. Liu, K. Schweda, and N. Xu, *Phys. Rev. C* **68**, 034910 (2003).  
 [15] S.F. Biagi, S.F. Biagi, M. Bourquin, A.J. Britten, R.M. Brown, H. Burckhart, A.A. Carter, J.R. Carter, Ch. Dore, P. Extermann, M. Gaillard, C.N.P. Gee, W.M. Gibson, J.C. Gordon, R.J. Gray, P.Igo-Kemenes, W.C. Louis, T. Modis, P.Muhlemann, J. Perrier, Ph. Rosset, B.J. Saunders, P. Schirato, H.W. Siebert, V.J. Smith, D.P. Stickland, K.-P. Streit, J.J. Thresher, and R.Weill, *Nucl. Phys. B* **186**, 1 (1981).  
 [16] R.A. Muller, *Phys. Lett. B* **38**, 123 (1972).  
 [17] J. Rafelski and B. Müller, *Phys. Rev. Lett.* **48**, 1066 (1982) [Erratum: *Phys. Rev. Lett.* **56**, 2334 (1986)].  
 [18] P. Koch, B. Müller, and J. Rafelski, *Phys. Rep.* **142**, 167 (1986).  
 [19] P. Koch, B. Müller, and J. Rafelski, *Int. J. Mod. Phys. A* **32**, 1730024 (2017).  
 [20] C. Blume, *EPJ Web of Conferences* **171**, 03001 (2018).  
 [21] C.M. Ko, *EPJ Web of Conferences* **171**, 03002 (2018).  
 [22] S. Voloshin and Y. Zhang, *Z. Phys. C* **70**, 665 (1996).  
 [23] A.M. Poskanzer and S.A. Voloshin, *Phys. Rev. C* **58**, 1671 (1998).  
 [24] J. Y. Ollitrault, *Phys. Rev. D* **46**, 229 (1992).  
 [25] H. Sorge, *Phys. Lett. B* **402**, 251 (1997); *Phys. Rev. Lett.* **82**, 2048 (1999).  
 [26] P. Danielewicz, R.A. Lacey, P.B. Gossiaux, C. Pinkenburg, P. Chung, J.M. Alexander, and R.L. McGrath, *Phys. Rev. Lett.* **81**, 2438 (1998).  
 [27] B. Zhang, M. Gyulassy, and C.M. Ko, *Phys. Lett. B* **455**, 45 (1999).  
 [28] V. Greco, C. M. Ko, and P. Lévai, *Phys. Rev. Lett.* **90**, 202302 (2003); *Phys. Rev. C* **68**, 034904 (2003).  
 [29] R. J. Fries, B. Müller, C. Nonaka, and S.A. Bass, *Phys. Rev. Lett.* **90**, 202303 (2003); *Phys. Rev. C* **68**, 044902 (2003).  
 [30] D. Molnar and S.A. Voloshin, *Phys. Rev. Lett.* **91**, 092301 (2003).  
 [31] R. Fries, V. Greco, and P. Sorensen, *Annu. Rev. Nucl. Part. Sci.* **58**, 177 (2008).  
 [32] R.C. Hwa and C.B. Yang, *Phys. Rev. C* **67**, 034902 (2003); **67**, 064902 (2003).  
 [33] J. Adams *et al.* [STAR Collaboration], *Phys. Rev. Lett.* **92**, 062301 (2004).  
 [34] J. Adams *et al.* [STAR Collaboration], *Phys. Rev. C* **72**, 014904 (2005).  
 [35] L.W. Chen, C.M. Ko, and Z.W. Lin, *Phys. Rev. C* **69**, 031901(R) (2004).  
 [36] P.F. Kolb, L.W. Chen, V. Greco, and C.M. Ko, *Phys. Rev. C* **69**, 051901(R) (2004).  
 [37] L.W. Chen and C.M. Ko, *Phys. Rev. C* **73**, 044903 (2006).  
 [38] J. Adams *et al.* [STAR Collaboration], *Phys. Rev. Lett.* **92**, 182301 (2004).  
 [39] J. Adams *et al.* [STAR Collaboration], *Phys. Rev. Lett.* **95**, 122301 (2005).  
 [40] C. Alt *et al.* [NA49 Collaboration], *Phys. Rev. Lett.* **94**, 192301 (2005).  
 [41] B.I. Abelev *et al.* [STAR Collaboration], *Phys. Rev. Lett.* **99**, 112301 (2007).  
 [42] B. Abelev *et al.* [ALICE Collaboration], *Phys. Lett. B* **728**, 216 (2014) [Erratum: *Phys. Lett. B* **734**, 409 (2014)].  
 [43] B. Abelev *et al.* [ALICE Collaboration], *Phys. Rev. C* **91**, 024609 (2015).  
 [44] B. Abelev *et al.* (ALICE Collaboration), *J. High Energy*

- Phys. **06**, 190 (2015).
- [45] L. Adamczyk *et al.* [STAR Collaboration], Phys. Rev. C **93**, 021903(R) (2016).
- [46] L. Adamczyk *et al.* [STAR Collaboration], Phys. Rev. Lett. **116**, 062301 (2016).
- [47] J.H. Chen, Y.G. Ma, G.L. Ma, X.Z. Cai, Z.J. He, H.Z. Huang, J.L. Long, W.Q. Shen, C. Zhong, and J.X. Zuo, Phys. Rev. C **74**, 064902 (2006).
- [48] F. Jin, D. Gangadharan, X.Z. Cai, H.Z. Huang, and Y.G. Ma, Phys. Rev. C **78**, 034907 (2008).
- [49] H.Z. Huang, J. Phys. G **36**, 064008(8PP) (2009).
- [50] M. He, R. J. Fries, and R. Rapp, Phys. Rev. C **82**, 034907 (2010).
- [51] S. Choudhury, D. Sarkar, and S. Chattopadhyay, Phys. Rev. C **95**, 024904 (2017).
- [52] Y.J. Ye, J. H. Chen, Y. G. Ma, S. Zhang, and C. Zhong, Chin. Phys. C **41**, 084101 (2017).
- [53] X.H. Jin, J.H. Chen, Y.G. Ma, S. Zhang, C.J. Zhang, and C. Zhong, Nucl. Sci. Tech. **29**, 54 (2018).
- [54] Z.W. Lin, C.M. Ko, B.A. Li, B. Zhang, and S. Pal, Phys. Rev. C **72**, 064901 (2005).
- [55] C. B. Dover, U. Heinz, and E. Schnedermann, Phys. Rev. C **44**, 1636 (1991).
- [56] F. Retière and M.A. Lisa, Phys. Rev. C **70**, 044907 (2004).
- [57] K.J. Sun and L.W. Chen, Phys. Lett. B **751**, 272 (2015).
- [58] K.J. Sun and L.W. Chen, Phys. Rev. C **93**, 064909 (2016).
- [59] K.J. Sun and L.W. Chen, Phys. Rev. C **94**, 064908 (2016).
- [60] H. Sato and K. Yazaki, Phys. Lett. B **98**, 153 (1981).
- [61] G.P. Lepage, J. Comp. Phys. **27**, 192 (1978).
- [62] R. Mattiello, H. Sorge, H. Stocker, and W. Greiner, Phys. Rev. C **55**, 1443 (1997).
- [63] K.J. Sun and L.W. Chen, Phys. Rev. C **95**, 044905 (2017).
- [64] S.S. Adler *et al.* [PHEHIX Collaboration], Phys. Rev. C **69**, 034909 (2004).
- [65] E. Schnedermann, J. Sollfrank, and U. Heinz, Phys. Rev. C **48**, 2462 (1993).